An Integrated Approach toward Retrieving Physically Consistent Profiles of Temperature, Humidity, and Cloud Liquid Water

ULRICH LÖHNERT, SUSANNE CREWELL, AND CLEMENS SIMMER

Meteorological Institute, University of Bonn, Bonn, Germany

(Manuscript received 29 October 2003, in final form 12 March 2004)

ABSTRACT

A method is presented for deriving physically consistent profiles of temperature, humidity, and cloud liquid water content. This approach combines a ground-based multichannel microwave radiometer, a cloud radar, a lidar-ceilometer, the nearest operational radiosonde measurement, and ground-level measurements of standard meteorological properties with statistics derived from results of a microphysical cloud model. All measurements are integrated within the framework of optimal estimation to guarantee a retrieved profile with maximum information content. The developed integrated profiling technique (IPT) is applied to synthetic cloud model output as a test of accuracy. It is shown that the liquid water content profiles obtained with the IPT are significantly more accurate than common methods that use the microwave-derived liquid water path to scale the radar reflectivity profile. The IPT is also applied to 2 months of the European Cloud Liquid Water Network (CLIWA-NET) Baltic Sea Experiment (BALTEX) BRIDGE main experiment (BBC) campaign data, considering liquid-phase, nonprecipitating clouds only. Error analysis indicates root-mean-square uncertainties of less than 1 K in temperature and less than 1 g m^{-3} in humidity, where the relative error in liquid water content ranges from 15% to 25%. A comparison of the vertically integrated humidity profile from the IPT with the nearest operational radiosonde shows an acceptable bias error of 0.13 kg m^{-2} when the Rosenkranz gas absorption model is used. However, if the Liebe gas absorption model is used, this systematic error increases to -1.24 kg m^{-2}, showing that the IPT humidity retrieval is significantly dependent on the chosen gas absorption model.

1. Introduction

A high temporal and spatial density of measurements providing continuous and accurate profiles of temperature, humidity, and hydrometeor size distribution is a major desire of the atmospheric modeling and meteorological satellite community. Such data would be extremely important for evaluating and improving model forecasts, parameterization schemes, and satellite retrieval algorithms. Radiosonde measurements are still the most important input for weather forecast models, despite their many disadvantages, for instance low temporal resolution (operationally 4 day^{-1} at maximum), erroneous measurements especially of humidity (Revercombe et al. 2003), the inability to measure the hydrometeor distribution, and their extremely high (manpower) costs. Strong efforts have been undertaken in the last four decades to develop alternative, ground-based instruments for continuously monitoring the vertical structure of the atmosphere. Different types of active and passive remote sensors have evolved that measure in different parts of the electromagnetic spectrum (e.g., microwave, infrared, and solar range). Since the interaction of atmospheric constituents with atmospheric radiation changes with wavelength, spectrally diverse measurements contain different information about the atmospheric composition. For both research and operational applications great interest resides in the knowledge of optimal instrument combination and the actual information content that can be gained from existing combined systems.

Combining measurements of different spectral characteristics and physical principles yields more accurate information than do single instrument retrievals. Stankov (1998) obtained sophisticated retrievals of atmospheric temperature and humidity profiles combining passive and active remote sensing systems with in situ measurements. This study employed lidar-ceilometer, satellite, global positioning system, wind profiler/radio acoustic sounding system (RASS), and commercial airliner data. Westwater (1997) notes that in addition to the combination of remote sensors, the inclusion of in situ measurements leads to improved results. Such measurements are needed, for example, when using Raman lidar to obtain humidity profiles (Han et al. 1994). An integrated technique to obtain tropospheric water vapor and cloud liquid water is presented by Han and Westwater (1995). In this paper ground-level measurements of

Corresponding author address: Dr. Ulrich Löhnert, Meteorological Institute, University of Munich, Theresienstr. 37, 80333 Munich, Germany.
E-mail: ulrich.loehnert@meteo.physik.uni-muenchen.de

temperature, humidity, and pressure are combined with a lidar-ceilometer, RASS, and microwave radiometer measurements within a retrieval based on radiosonde statistics.

When a microwave radiometer and a cloud radar are collocated, both measurements can be combined to successfully derive the liquid water content (LWC) profile (Frisch et al. 1998). Two- or three-channel *microwave radiometers* play a central role in retrievals of the cloudy atmosphere because of the semitransparency of clouds in the microwave spectral region. Recent developments include a sophisticated retrieval by Liljegren et al. (2001), who have developed a statistical, site-independent dual-channel retrieval to derive LWP with improved accuracy. Microwave radiometers with multiple frequencies (*radiometric profilers*) have the potential to derive temperature and humidity profiles (Solheim et al. 1998) and measure the liquid water path (LWP) with a higher accuracy than two-channel radiometers (Crewell and Löhnert 2003). *Cloud radars* can be used to gain insight into the vertical position and structure of the cloud. However, they provide only very limited information on cloud microphysical parameters because of the fact that the measured quantity, radar reflectivity (Z), is proportional to the sixth moment of the cloud drop size distribution.

In this study optimal estimation theory (Rodgers 2000) is applied to simultaneously retrieve profiles of temperature, humidity, and LWC. Optimal estimation retrievals have been developed to derive temperature and humidity profiles from space (Lerner et al. 2002). Löhnert et al. (2001) describe an optimal estimation technique to retrieve LWC profiles from ground-based Z measurements of a cloud radar and microwave radiometer–derived LWP. In the following paper, the integrated profiling technique (IPT) is presented, which explicitly combines 19 microwave brightness temperature measurements with 95-GHz cloud radar measurements, lidar-ceilometer cloud-base measurements, ground-level measurements of temperature, humidity, and pressure, nearest radiosonde profiles, and an LWC a priori profile obtained from statistics of a microphysical cloud model. The measurement techniques and the instruments employed, as well as the cloud model are briefly described in section 2 of this paper. Section 3 gives an overview of how the single measurements are embedded within the optimal estimation formulation. Two explicit formulations of the IPT are derived. The first formulation corresponds to an idealized case with given temperature (T), absolute humidity (q), and pressure (p) (IPT-a). The second formulation assumes that p is given and T and q are only accessible as statistical a priori information (IPT-b). Consequently T and q are derived within the retrieval procedure. To assess the accuracy of the retrieval method, the IPT-a is applied to synthetic cloud model output in section 4. To show the benefits of the IPT, the retrieval results are compared with a standard retrieval method. In section 5 the IPT-b is applied to real observations collected during the third extensive operation period of the European Cloud Liquid Water Network (CLIWA-NET) project (Crewell et al. 2003) at Cabauw, Netherlands, from 1 August to 30 September 2001. To obtain an error estimate of the IPT, theoretical accuracies are evaluated for each retrieved profile. Also, the sensitivity of the retrieved LWP and the sensitivity of the retrieved vertical structure of water vapor and temperature in relation to two different, but common microwave gas absorption models are examined. The last section wraps up the most important results and discusses IPT extensions toward an ''all-encompassing'' algorithm.

2. Measurement and instrument description

The measurements described in the following were all carried out within the European fifth framework project CLIWA-NET at the Cabauw Experimental Site for Atmospheric Research (CESAR) facility in the Netherlands. The measurements were part of the Baltic Sea Experiment (BALTEX) BRIDGE main experiment (BBC) and took place from 1 August to 30 September 2001. The measurements of the following instruments as well as the output of the depicted microphysical cloud model, which can be interpreted as a virtual measurement, are later used as input for the IPT.

a. Cloud radar

The 95-GHz cloud radar Microwave Radar for Cloud Layer Exploration (MIRACLE; Danne et al. 1999) of GKSS, Germany, is used in this study. MIRACLE observes vertical profiles of Z, Doppler velocity (v_D), and Doppler velocity spectral width. Here, Z is evaluated starting at 500 m above ground level in order to exclude near-field effects. Because of its polarimetric characteristics MIRACLE can also derive the linear depolarization ratio (LDR) with a threshold of -26 dB, yielding information on the presence of ice particles in the cloud. The MIRACLE data for the BBC campaign are available with a temporal resolution of 5 s. In this study, however, the time series were only evaluated for every fourth MIRACLE measurement to reduce computing time. The vertical resolution of the MIRACLE measurements is mostly 82.5 m, except on days with thin low-level liquid clouds, when the vertical resolution was increased to 37.5 m.

b. Microwave radiometer

The 22-channel microwave profiler Microwave Radiometer for Cloud Cartography (MICCY; Crewell et al. 2001) from the University of Bonn, Germany, performs simultaneous measurements of microwave brightness temperatures in three bands covering distinct atmospheric absorption characteristics in the range of 20–90 GHz (Fig. 1). In this study we only use 19 of the

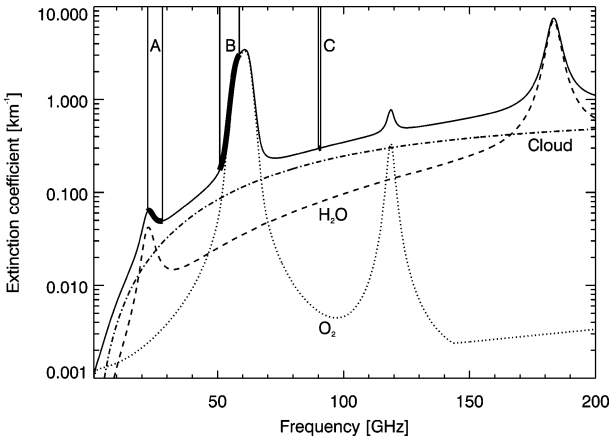

FIG. 1. Microwave extinction spectrum at 850 hPa derived from the Cabauw radiosonde at 1100 UTC 1 Aug 2001. The dashed line shows the water vapor contribution, the dotted line the oxygen contribution, and the dotted–dashed line the theoretical cloud liquid contribution of a cloud with 0.2 g m^{-3} LWC (relative humidity was above 95% at 850 hPa). The solid line is the sum of all contributions and the intervals indicated by A, B, and C show the measurement bands of the microwave radiometer MICCY.

22 channels because of the fact that three channels measure at the same frequency, but with perpendicular polarization. Because of the increase of pressure broadening with decreasing height at the water vapor line at 22.235 GHz and at the oxygen absorption complex around 60 GHz, profile information may be obtained on q and T, respectively. The increasing absorption of liquid water with increasing frequency also allows an accurate determination of total cloud liquid water, especially when the highly liquid water sensitive 90-GHz channel is included (Löhnert and Crewell 2003). The temporal resolution during the BBC campaign was 1 s. Every 4 min an internal gain calibration was performed with a duration of ~15 s.

c. Lidar-ceilometer

A standard Vaisala, Inc., CT-75K lidar-ceilometer with a temporal resolution of 15 s is used to detect cloud base. Lidar-ceilometers operate according to the same principle as radars, but in the optical region. The backscattered radiation is, however, proportional to the droplet diameter squared (optical regime) because of the wavelength being much shorter than the particle diameter. Accordingly, typical lidar-ceilometers are more sensitive to small cloud particles than cloud radars, which in turn are highly sensitive to larger drops. Thus, lidar-ceilometer measurements are more accurate in deriving the actual cloud-base height while cloud radars often detect light drizzle with negligible LWC below the actual cloud base. Also, often cloud radars are not sensitive enough to detect small droplets occurring in developing cumulus, which are, however, usually captured by lidar-ceilometers. Generally lidar-ceilometers cannot be used to detect the vertical cloud structure because most liquid water clouds are optically thick in the optical region of the spectrum such that the lidar-ceilometer signal will almost always be extinguished in the lower part of the cloud.

d. Radiosonde and ground-level measurements

The profiles of T, q, and p from the nearest (~30 km distance) operational radiosonde site De Bilt, Netherlands, are used as additional information when the IPT is applied to real measurements. Radiosonde launches were performed every day at 0000, 0600, 1200, and 1800 UTC. Ground-level measurements of temperature (T_{gr}) and humidity (q_{gr}) available directly at the measurement site are used to constrain the algorithm at the lowest level.

e. Microphysical cloud model

The statistics of a single-column, dynamical, spectrally resolved microphysical cloud model (DCM; Issig 1997) are interpreted as an additional, virtual measurement within the IPT. For given profiles of T, q, and p the DCM predicts liquid drop size spectra for 40 logarithmically scaled radius intervals with 250-m vertical resolution up to a height of 10 km. Results are recorded every 40 s of the simulation time for a duration of 2 h after initialization. A more detailed DCM description is given in Löhnert et al. (2001).

To create a representative dataset, 1 yr of radiosonde data (1990) is used as DCM input originating from the station Essen (at a distance of ~200 km from Cabauw) of the German Weather Service. For every DCM run, each model output time step is examined at each height below 5 km for the presence of liquid clouds. The threshold to be exceeded in LWC to analyze a cloud is set to 0.005 g m^{-3}. Using all model runs, mean LWC profiles and corresponding covariance matrices are calculated for six separate vertical cloud extensions from 250 m minimum to 1500 m maximum cloud depth. It is assumed that these six profiles and their covariances represent continental shallow cumulus and stratocumulus clouds in an adequate way. Drizzling cases are excluded when evaluating DCM output.

3. Sensor synergy

This section describes how the measurements mentioned earlier can be combined to give optimal estimates of the desired profiles of T, q, and LWC. Since a main objective of this study is to retrieve profiles of LWC, it is shown in section 3a how the IPT can be applied if in an ideal case the vertical distributions of T, q, and p are given (IPT-a). In section 3b we describe how IPT-b can be used to retrieve LWC profiles when T, q, and p are only available from the nearest operational radiosonde measurement. This approach encompasses a si-

multaneous retrieval of *T, q,* and LWC, where the pressure profile is assumed to be given exactly by the radiosonde and is consequently not retrieved.

Often *statistical* methods are useful when remote sensing retrievals are developed, especially when complex relationships with a large number of degrees of freedom are being studied. However, if physical knowledge of the radiation–atmosphere interaction is given, retrieval algorithms can be made *physically consistent* by means of a so-called *forward model.* In this context physically consistent means that the retrieved profile will reproduce the measured radiation within the measurement accuracy. In this study the microwave radiative transfer equation (e.g., Janssen 1993) and a relationship between *Z* and LWC are regarded as the valid forward model.

a. Inversion theory

Generally, the problem to be solved in remote sensing is an *ill-posed inverse problem.* This means that the forward model $\mathbf{y} = F(\mathbf{x})$ relating atmospheric parameters ($\mathbf{x}$) to measurements ($\mathbf{y}$) is well known in theory, but retrieving the parameters from the measurements is ambiguous. [Note that boldface parameters indicate profile (height dependent) or measurement (spectrally dependent) vectors from here onward.] The limited number of usually highly correlated and erroneous measurements $\mathbf{y}$ leads to a very large number of solutions that satisfy the measurements. The only way to solve this dilemma is to combine the measurements with auxiliary information.

Bayes's theorem (e.g., Rodgers 2000) provides a general formulation for the solution of noisy inverse problems. It describes the probability density function for all possible solutions $\mathbf{x}$ given the measurement $\mathbf{y}$

$$P(\mathbf{x}|\mathbf{y}) = \frac{P(\mathbf{y}|\mathbf{x})P(\mathbf{x})}{P(\mathbf{y})}, \tag{1}$$

with $P(\mathbf{x})$ and $P(\mathbf{y})$ stating the probability density functions (PDF) of the atmospheric profile and the measurement, respectively. The value $P(\mathbf{y}|\mathbf{x})$ is the conditional PDF of $\mathbf{y}$ given $\mathbf{x}$, which comprises the knowledge of the forward model and the measurement error, and $P(\mathbf{x})$ states some kind of a priori knowledge of atmospheric parameters, for example, climatological data or an analysis from a forecast model. The solution of Eq. (1), $P(\mathbf{x}|\mathbf{y})$, can be interpreted as an improvement of the a priori knowledge of $\mathbf{x}$, which can be achieved through combination with the knowledge about the atmospheric state obtained from the imperfect measurement $\mathbf{y}$. It is important to mention that Eq. (1) does not provide an explicit solution to the inverse problem, but rather classifies the possible solutions as more or less probable.

The IPT developed in this study uses the so-called optimal estimation equations, which can be directly derived from Bayes's theorem if the forward model is considered linear and the PDFs involved are assumed to be Gaussian. The formulation allows the incorporation of multiple measurements into the retrieval. Given a set of measurements, the optimal estimation inversion procedure finds a solution that satisfies the measurements after the forward model has been applied to the retrieved parameters. As a condition, the error characteristics of each measurement and of the forward model must be accurately described by covariance matrices. The degree to which each measurement is satisfied depends on the measurement error and the covariance matrices. This means that measurements with small errors and/or an accurate description of the relation between measurement and parameter will have a higher weight in the solution than measurements with large errors and/or an inaccurate description of the relationship between measurement and parameter.

If the forward model is moderately nonlinear, it can be simplified to a linear problem by means of a Taylor series expansion about an initial state vector $\mathbf{x}_i$. If higher terms are omitted, $\mathbf{y}$ can then be expressed by

$$\mathbf{y} = \mathbf{y}_i + \mathbf{K}_i(\mathbf{x} - \mathbf{x}_i), \tag{2}$$

with $\mathbf{K}_i = \partial\mathbf{F}/\partial\mathbf{x}_i$ denoting the Jacobi matrix of the problem.

In our case we are interested in deriving the parameter vector $\mathbf{x}$ consisting of the profiles of *T, q,* and LWC. The measurement vector $\mathbf{y}$ consists of 19 MICCY brightness temperatures, the radar reflectivity profile at ncld detected cloud levels, and the ground-level measurements of temperature and humidity ($T_{\rm gr}$, $q_{\rm gr}$):

$$\mathbf{y} = \begin{pmatrix} \mathrm{TB}_1 \\ \vdots \\ \mathrm{TB}_{19} \\ Z_1 \\ \vdots \\ Z_{\rm ncld} \\ T_{\rm gr} \\ q_{\rm gr} \end{pmatrix}. \tag{3}$$

Here $\mathbf{F}$ is then given by

$$\begin{aligned} \mathrm{TB}_1 &= \mathrm{RTO}(\mathbf{T, q, p, LWC},\ f_1) \\ &\vdots \\ \mathrm{TB}_{19} &= \mathrm{RTO}(\mathbf{T, q, p, LWC},\ f_{19}) \\ Z_1 &= a_1\mathrm{LWC}^{b_1} \\ &\vdots \\ Z_{\rm ncld} &= a_{\rm ncld}\mathrm{LWC}^{b_{\rm ncld}} \\ T_{\rm gr} &= T(1) \\ q_{\rm gr} &= q(1). \end{aligned} \tag{4}$$

The forward model performs the radiative transfer calculation (RTO is the radiative transfer operator, which

calculates the brightness temperatures TB from the given atmospheric state) at the 19 microwave frequencies f_i, $i \in [1, 2, \ldots, 19]$, converts LWC to Z via a power-law relationship at the ncld detected cloud levels and uses the ground-level measurements to constrain the solution. The RTO performs the microwave radiative transfer only for nonscattering cases. This approximation is justified for nonprecipitating clouds and frequencies below ~100 GHz (Simmer 1994). Unless stated otherwise, microwave absorption for water vapor and oxygen is calculated according to Rosenkranz (1998) and for liquid water according to Liebe et al. (1993).

In order to constrain the solution to sensible profiles we use a priori information ($\mathbf{x}_a$) of **T** and **q** from the nearest operational radiosonde ascent (section 3c) and of **LWC** from mean DCM profiles (section 3b).

Following Rodgers (2000), the optimal estimation equation for our problem can be written as

$$\mathbf{x}_{i+1} = \mathbf{x}_i + (\mathbf{K}_i^{\mathrm{T}}\mathbf{S}_e^{-1}\mathbf{K}_i + \mathbf{S}_a^{-1})^{-1} \times [\mathbf{K}_i^{\mathrm{T}}\mathbf{S}_e^{-1}(\mathbf{y} - \mathbf{y}_i) + \mathbf{S}_a^{-1}(\mathbf{x}_i - \mathbf{x}_a)], \quad (5)$$

where i represents the iteration step, $\mathbf{S}_e$ is the combined measurement and forward model error covariance matrix, and $\mathbf{S}_a$ is the a priori covariance matrix. We assume that temperature and humidity represent Gaussian-distributed parameters, that random errors prevail in the TB and the errors of Z in the units of dBZ are also Gaussian-distributed. However, LWC is clearly not Gaussian-distributed. To be able to apply Eq. (5) nevertheless, we retrieve 10 $\log_{10}$(LWC) which more closely resembles a Gaussian-distributed parameter than LWC. In the following the term LWC will refer to 10 $\log_{10}$(LWC) unless stated otherwise.

In this study $\mathbf{K}_i$ is recalculated after each iteration step. Equation (5) is iterated i_{op} times in i until an adequate minimum of a cost function is found, yielding the solution $\mathbf{x}_{\mathrm{op}}$. Rodgers (2000) describes a method to judge whether the iteration procedure has reached convergence by considering a quadratic cost function between $F(\mathbf{x}_i)$ and $F(\mathbf{x}_{i+1})$:

$$[F(\mathbf{x}_{i+1}) - F(\mathbf{x}_i)]^{\mathrm{T}}\mathbf{S}_{\delta y}^{-1}[F(\mathbf{x}_{i+1}) - F(\mathbf{x}_i)] \ll d, \quad (6)$$

with d denoting the dimension of **y** and $\mathbf{S}_{\delta y}$ is the covariance matrix between the measurement **y** and $F(\mathbf{x}_{\mathrm{op}})$. It is important to note that the solution $\mathbf{x}_{\mathrm{op}}$ must be interpreted as the most probable solution of a Gaussian-distributed probability density function, whose covariance can be written as

$$\mathbf{S}_{\mathrm{op}} = (\mathbf{K}_{i_{\mathrm{op}}}^{\mathrm{T}}\mathbf{S}_e^{-1}\mathbf{K}_{i_{\mathrm{op}}} + \mathbf{S}_a^{-1})^{-1}. \quad (7)$$

The diagonal elements of this matrix give an estimate of the mean quadratic error of $\mathbf{x}_{\mathrm{op}}$.

Because the microwave signal is dominated by signals from the lower troposphere, the vertical resolution of T and q is chosen to be 250 m in the lowest 5 km, 500 m from 5 to 10 km, and 5000 m from 10 to 30 km. Climatological radiosonde data are used as profile extension for T above 10 km and q is set to zero above this level. Although most atmospheric moisture is below 10 km, it is necessary to include temperature information up to 30 km, since neglecting this information can lead to TB offsets on the order of 5 K in the 50-GHz region.

b. IPT with given T, q, and p (IPT-a)

In the ideal case when profiles of T, q, and p are given, **x** only consists of the LWC profile, $\mathbf{x}_a$ is the mean LWC model profile of all calculated DCM clouds with vertical extent of ncld × 250 m with ncld ∈ [1, 2, . . . , 6], and consequently $\mathbf{S}_a$ takes the form

$$\mathbf{S}_a = \begin{pmatrix} c_{1,1}^{\mathrm{LWC}} & \vdots & c_{1,\mathrm{ncld}}^{\mathrm{LWC}} \\ \vdots & \vdots & \vdots \\ c_{\mathrm{ncld},1}^{\mathrm{LWC}} & \vdots & c_{\mathrm{ncld},\mathrm{ncld}}^{\mathrm{LWC}} \end{pmatrix}. \quad (8)$$

This formulation depicts the covariance matrix for a cloud with ncld levels, where $c_{i,j}^{\mathrm{LWC}}$ ($i, j \in [1, 2, \ldots,$ ncld]) denotes the covariance between LWC at cloud level i and j above cloud base. The measurement vector is reduced to **TB** and **Z**, and $\mathbf{S}_e$ is then given by

$$\mathbf{S}_e = \begin{pmatrix} \varepsilon_1^{\mathrm{TB}} & 0 & 0 & 0 & 0 & 0 \\ 0 & \vdots & 0 & 0 & 0 & 0 \\ 0 & 0 & \varepsilon_{19}^{\mathrm{TB}} & 0 & 0 & 0 \\ 0 & 0 & 0 & \varepsilon_{1,1}^{\mathrm{dBZ}} & \vdots & \varepsilon_{1,\mathrm{ncld}}^{\mathrm{dBZ}} \\ 0 & 0 & 0 & \vdots & \vdots & \vdots \\ 0 & 0 & 0 & \varepsilon_{\mathrm{ncld},1}^{\mathrm{dBZ}} & \vdots & \varepsilon_{\mathrm{ncld},\mathrm{ncld}}^{\mathrm{dBZ}} \end{pmatrix}. \quad (9)$$

Here, $\varepsilon_{f_i}^{\mathrm{TB}}$ with $f_i \in [1, 2, \ldots, 19]$ represents the squared TB error for each frequency due to calibration *and* forward model. In a first, reasonable assumption the TB errors are not correlated, which means that the off-diagonal matrix elements are zero in this part of $\mathbf{S}_e$. Random calibration accuracy may be described by an error of 0.5 K (Crewell et al. 2001), whereby no systematic calibration errors are assumed to exist. Forward model errors are mostly due to uncertainties in simulating microwave absorption (Kuhn 2003) for which, unfortunately, still no reliable evaluations exist. Since the gas absorption models according to Liebe et al. (1993, hereinafter L93) and Rosenkranz (1998, hereinafter R98) are considered as standard up-to-date absorption models (T. Kuhn 2003, personal communication), the variances between these two models are regarded as part of the $\varepsilon_{f_i}^{\mathrm{TB}}$. The systematic differences are subtracted before calculating $\mathbf{S}_e$ (see Fig. 2). Unknown systematic errors, which may cause retrieval bias errors when applying algorithms to real measurements, also cannot be included in $\mathbf{S}_e$. The impact of the systematic absorption model differences to the IPT retrieval results are shown later in section 6b. Note that absorption model errors will not exist when applying IPT to model data because the TBs are simulated consistently with one and the same RTO. In this case (i.e., application to simulated

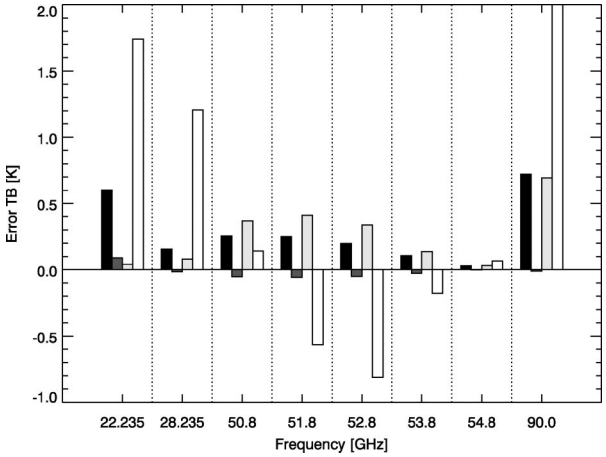

FIG. 2. Performance characteristics of the FAP for eight selected MICCY frequencies. The black bars indicate the rms error between the FAP-derived brightness temperatures and the exact calculations, whereas the dark gray bars show the corresponding (negligible) bias errors (FAP − R98). The light gray bars indicate the rms differences between the L93 and R98 gas absorption models, and the white bars are the systematic differences (L93 − R98). The systematic difference between both models is 5.3 K at 90 GHz.

measurements; see section 4), $\varepsilon_{f_i}^{\mathrm{TB}}$ only consists of the assumed random calibration error.

The $\varepsilon_{i,j}^{\mathrm{dBZ}}$ represent the error covariances of Z between cloud levels i and j and consist of the errors due to random radar calibration uncertainty (~3 dBZ; Danne et al. 1999), errors in the Z–LWC relationship, and errors due to the attenuation correction scheme. The latter two have been derived by simulating Z from DCM drop size distributions and are described by Löhnert et al. (2001). Additionally, the attenuation correction scheme has been expanded in order to correct for attenuation due to water vapor.

c. IPT with T and q as a priori (IPT-b)

In this case $\mathbf{x}$ consists of the profiles of T, q, and LWC and the a priori profile $\mathbf{x}_a$ is obtained from a linearly interpolated estimate of temperature and humidity between two consecutive ascents of the nearest operational radiosonde site. In the case of the BBC campaign, the operational site DeBilt is located at a distance of approximately 30 km to the measurement site Cabauw. At the beginning of the BBC campaign 35 radiosondes were launched at the Cabauw site. These are used to evaluate the interpolated estimates from De Bilt in order to construct the error covariance matrix $\mathbf{S}_a$ for T and q. The LWC a priori information is again taken from the DCM output. We can now write the full covariance matrix $\mathbf{S}_a$ as

$$\mathbf{S}_a = \begin{pmatrix} c_{1,1}^{\mathrm{T,T}} & \cdots & c_{1,n}^{\mathrm{T,T}} & c_{1,1}^{\mathrm{T},q} & \cdots & c_{1,n}^{\mathrm{T},q} & c_{1,1}^{\mathrm{T,LWC}} & \cdots & c_{1,\mathrm{ncld}}^{\mathrm{T,LWC}} \\ \vdots & \vdots & \vdots & \vdots & \vdots & \vdots & \vdots & \vdots & \vdots \\ c_{n,1}^{\mathrm{T,T}} & \cdots & c_{n,n}^{\mathrm{T,T}} & c_{n,1}^{\mathrm{T},q} & \cdots & c_{n,n}^{\mathrm{T},q} & c_{n,1}^{\mathrm{T,LWC}} & \cdots & c_{n,\mathrm{ncld}}^{\mathrm{T,LWC}} \\ c_{1,1}^{q,\mathrm{T}} & \cdots & c_{1,n}^{q,\mathrm{T}} & c_{1,1}^{q,q} & \cdots & c_{1,n}^{q,q} & c_{1,1}^{q,\mathrm{LWC}} & \cdots & c_{1,\mathrm{ncld}}^{q,\mathrm{LWC}} \\ \vdots & \vdots & \vdots & \vdots & \vdots & \vdots & \vdots & \vdots & \vdots \\ c_{n,1}^{q,\mathrm{T}} & \cdots & c_{n,n}^{q,\mathrm{T}} & c_{n,1}^{q,q} & \cdots & c_{n,n}^{q,q} & c_{n,1}^{q,\mathrm{LWC}} & \cdots & c_{n,\mathrm{ncld}}^{q,\mathrm{LWC}} \\ c_{1,1}^{\mathrm{LWC,T}} & \cdots & c_{1,n}^{\mathrm{LWC,T}} & c_{1,1}^{\mathrm{LWC},q} & \cdots & c_{1,n}^{\mathrm{LWC},q} & c_{1.1}^{\mathrm{LWC,LWC}} & \cdots & c_{1,\mathrm{ncld}}^{\mathrm{LWC,LWC}} \\ \vdots & \vdots & \vdots & \vdots & \vdots & \vdots & \vdots & \vdots & \vdots \\ c_{\mathrm{ncld},1}^{\mathrm{LWC,T}} & \cdots & c_{\mathrm{ncld},n}^{\mathrm{LWC,T}} & c_{\mathrm{ncld},1}^{\mathrm{LWC},q} & \cdots & c_{\mathrm{ncld},n}^{\mathrm{LWC},q} & c_{\mathrm{ncld},1}^{\mathrm{LWC,LWC}} & \cdots & c_{\mathrm{ncld,ncld}}^{\mathrm{LWC,LWC}} \end{pmatrix}. \quad (10)$$

Here, the $c_{i,j}$ with $i, j \in [1, 2, \ldots, n]$ represent the error covariance between height level i and j for the parameters specified in the upper subscripts. Note that $n = 35$ is the number of layers for the T and q retrieval, whereas the LWC contributions are only calculated within the cloud at ncld $\in [1, 2, \ldots, 6]$ levels.

For IPT-b the measurement vector $\mathbf{y}$ corresponds to the formulation in Eq. (3) and the error covariance matrix $\mathbf{S}_e$ has the same structure as Eq. (9), except that it is extended to include the expected error of ground-level T (0.5 K) and q (0.5 g m^{-3}) measurement. Last, within the cloud boundaries, IPT-b constrains q to its saturation value at each iteration step with the corresponding T. For each iteration, the Jacobi matrix $\mathbf{K}_i$ is calculated as $\partial\mathbf{F}/\partial\mathbf{x}_i$ where each TB derivative must be determined with respect to T, q, and LWC at each height. Considering the vertical discretization and the fact that $\mathbf{K}_i$ is calculated numerically results in relatively long computing times (~30 s for one iteration on a standard PC).

The limiting time factor when calculating $\mathbf{K}_i$ is the time for determining the absorption coefficient due to water vapor and oxygen. As a consequence a fast absorption predictor (FAP) is developed for the 19 MICCY frequencies based on the R98 absorption model. The total absorption coefficient abs (f_i) for water vapor and

oxygen is calculated as a function of T, q, and p in the following way:

$$\begin{aligned}\text{abs}(f_i) = {} & m_{0,i} + m_{1,i}T + m_{2,i}T^2 + m_{3,i}T^3 \\ & + m_{4,i}q + m_{5,i}q^2 + m_{6,i}q^3 \\ & + m_{7,i}p + m_{8,i}p^2 + m_{9,i}p^3. \qquad (11)\end{aligned}$$

The m coefficients are derived by means of multiple linear regression. Four years (1990–93) of radiosonde ascents started 2 times per day (0000 and 1200 UTC) from the station De Bilt, Netherlands, are used to calculate the absorption coefficient at each height level. Then a least squares minimization is performed to derive the m coefficients for each MICCY frequency f_i. The ascents of the years 1994–97 are used as a testing dataset to determine how well such a simple model can reproduce the model ''truth.'' Figure 2 shows that a forward model with FAP is able to reproduce the TB with overall accuracies better than 0.7 K. The root-mean-square (rms) difference (bias free) between the L93 and R98 model is even higher than the random FAP error at frequencies 50.8–53.8 GHz. Note the enormous systematic differences between L93 and R98 at 22.235 and 90 GHz. Applying FAP within the IPT improves computing time of $\mathbf{K}_i$ by a factor of 5. Here, **T** and **q** can also be described by means of empirical orthogonal functions (EOF; e.g., Simmer 1994). Using the DeBilt radiosonde data **T** and **q** can be optimally described with nine and five EOFs, respectively. With this data reduction, computing time is again reduced approximately by a factor of 4. However, the retrieved profiles of q often show unrealistic jumps and edges owing to the data reduction. For this reason the EOF approach is not further pursued in this study.

4. Algorithm application to cloud model output

To evaluate the IPT performance for deriving LWC profiles, we apply the IPT-a version to the DCM output, for instance assuming that T, q, and p are given (see section 3b). This idealized assumption provides information on the maximum degree of LWC accuracy which may be achieved with the IPT. The direct incorporation of T, q, and p is one of the major benefits of the IPT in comparison with other LWC profiling methods with microwave radiometer and radar. The retrieval product will be more accurate in terms of LWC because of the fact that, even during the presence of clouds, microwave brightness temperatures are to a high degree determined by the temperature and humidity profile.

To analyze the benefits of single-measurement components, the IPT-a is modified to be applied to the DCM output without the use of cloud radar or microwave radiometer data, respectively. The first modification (IPT-MWR) only uses the TB and the given cloud boundaries, thus neglecting the Z–LWC information, whereas the second modification (IPT-RAD) uses the Z–LWC relationship without the TB measurements (Fig. 3). For both algorithms the measurement vector **y** and the matrix $\mathbf{S}_e$ are modified correspondingly. Both IPT-MWR and IPT-RAD use the LWC a priori profile as an additional virtual measurement.

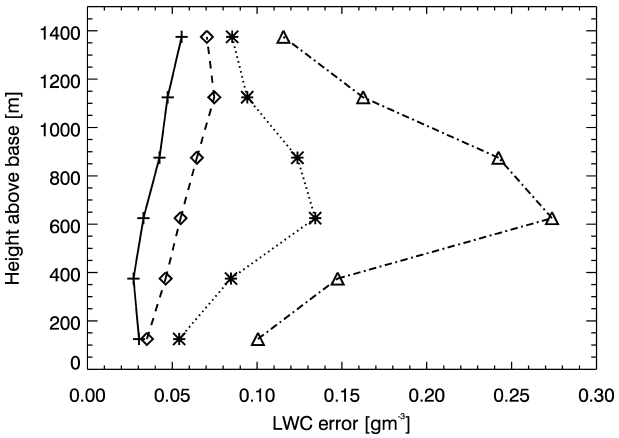

FIG. 3. The rms errors of different LWC algorithms applied to the DCM output. The crosses indicate the IPT-a errors at each height above base level. Also shown are algorithm errors resulting from the exclusion of microwave data (IPT-RAD, stars) and exclusion of the radar data (IPT-MWR, diamonds). The triangles indicate the results when only the radar reflectivities are used to infer LWC.

a. Discussion

When regarding the errors in Fig. 3 it seems obvious that the Z–LWC relationship alone is not well suited to derive LWC profiles. In case the cloud boundaries can be determined, the IPT-MWR adds more information to the vertical distribution of LWC than the IPT-RAD. It is clear that, on the one hand, the IPT-RAD algorithm is only poorly suited for retrieving LWC most probably due to the fact that Z is proportional to the droplet diameter to the power of 6 and LWC to the droplet diameter to the power of 3. The IPT-MWR algorithm on the other hand, quite accurately derives the total amount of liquid water and is capable of retrieving fairly accurate LWC profiles when a representative LWC a priori profile is given. Figure 3 also makes clear that combining both microwave radiometer and cloud radar is complementary and significantly increases the accuracy in comparison with the cases when only one instrument is used alone. Thus, both instruments should definitely be located next to each other when profiling LWC.

b. Comparison with other algorithms

To show the benefits of the IPT, we compare the IPT-a version with a standard LWC profiling approach, in which the microwave-derived LWP is used to scale the Z–LWC relationship (e.g., Frisch et al. 1998; Ovtchinnikov and Kogan 2000). To simulate measurement errors in LWP for a standard two-channel microwave ra-

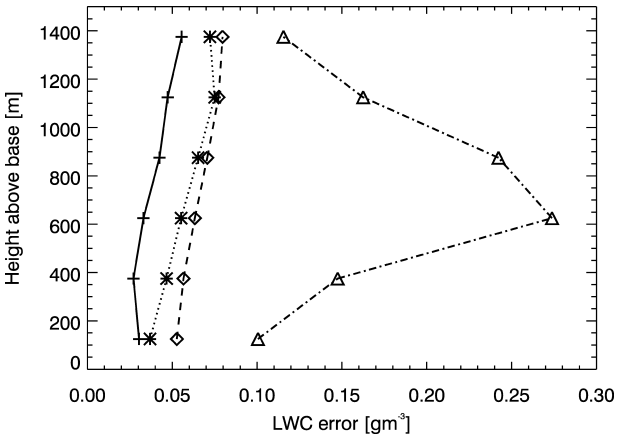

FIG. 4. IPT-a rms errors (crosses) in comparison with the model-derived *Z*–LWC relation scaled to LWP with a random accuracy of 10 (stars) and 30 (diamonds) g m^{-2}. Also shown (as in Fig. 3) is the accuracy of the *Z*–LWC relation without scaling (triangles).

diometer, Gaussian random noise with standard deviations of 10 and 30 g m^{-2} was added to the model-calculated values. In this context 30 g m^{-2} must be seen as a realistic error estimate for standard two-channel microwave radiometers for LWP values ranging up to 500 g m^{-2}. The 10 g m^{-2} error assumption is optimistic. These algorithms are then applied to the same DCM output as in section 3a (Fig. 4). Again it can be seen that the accuracies of the pure *Z*–LWC relation are much lower than those of the other methods. Obviously the IPT-a version is even more accurate than the optimistic (10 g m^{-2}) error approach. The reasons for this are the incorporation of the hypothetically given *T*, *q*, and *p* profiles and the direct inclusion of all 19 brightness temperatures, which avoids LWP retrieval errors.

5. Algorithm application to real data

The IPT is now applied to time series of measurements obtained during the BBC campaign in August and September 2001 at the Cabauw site. Since temperature and humidity profiles can only be estimated from nearby radiosonde ascents, these profiles are now included as *a priori information* (IPT-b, see section 3c) and are retrieved together with the LWC profiles. To determine the cloud boundaries most accurately, lidar-ceilometer measurements are used to obtain cloud base and the highest reflectivity bin of the cloud radar with a significant signal-to-noise-ratio is used as cloud top. To be able to apply the IPT, the radar reflectivities (on their original resolution) are averaged to the IPT resolution of 250 m. Cloud-base height is also brought to the 250-m grid by locating the closest 250-m level.

a. Adaptation to radar range resolution

In its form described in section 3c, the resulting LWC profiles will be retrieved with a vertical range resolution of 250 m. Most existing LWC retrieval algorithms retrieve LWC on the radar range resolution, especially when *Z*–LWC–based methods are used. The IPT results can be easily used to derive a product on radar range resolution. To achieve this, the original radar reflectivities (Z_{RR}) are scaled with the LWC retrieved by the IPT on the 250-m resolution:

$$\mathrm{LWC}_{RR}[h_{RR,i}(j)] = \frac{a_i Z_{RR}[h_{RR,i}(j)]^{b_i}}{\mathrm{LWC}_{IPT}[h_{IPT}(i)]}, \qquad (12)$$

where *h* denotes height, the indices RR and IPT are the radar and the IPT vertical range resolution, respectively, $i \in [1, 2, \ldots, \mathrm{ncld}]$ is the cloud height index within the IPT 250-m system, and *j* is the height index of the radar system within the *i*th IPT bin. All of the radar pixels Z_{RR} located within the bounds of the *i*th IPT height bin are converted to LWC by a scaled power law with the same coefficients *a* and *b* as in the formulation of the forward model [Eq. (4)]. Equation (12) scales by the same principle as the LWP-constrained LWC algorithm used in section 4b, only that here we constrain LWC_{RR} to LWC_{IPT} instead of LWC_{RR} to LWP. By first applying the IPT and subsequently using Eq. (12) we arrive at a product on the desired resolution, with an optimized LWC profile on a 250-m resolution, and a sophisticated LWC product on the original radar resolution.

b. Algorithm applicability

In order to apply the IPT to the BBC data, the microwave radiometer, cloud radar, and lidar-ceilometer measurements must be available simultaneously. A threshold time window of 20 s is chosen because the hot load calibration time of MICCY, which is performed every 4 min, has a duration of 15 s. The IPT is always applied at the radar measurement time. Within the time window, the closest measurement of MICCY and the lidar-ceilometer are identified and combined within the IPT.

Because the IPT in its present form can only be applied to nonprecipitating and purely liquid water cases, a cloud classification scheme was developed and applied to the BBC data. This enables automatic IPT application such that no restriction to case studies must be made. Within the classification scheme each radar pixel is classified into ''pure ice,'' ''pure liquid,'' ''mixed phase,'' or ''unclassified'' using the microwave-derived LWP, the nearest operational radiosonde measurements of *T*, lidar-ceilometer cloud base, radar reflectivity, and radar linear depolarization ratio (LDR). A direct indication for the presence of ice is an LDR larger than −26 dB. Because the MICCY microwave channels are intensitive to ice, cases with zero LWP and a detected cloud within the radar measurement are classified as pure ice. However, most cases are not that straightforward so that certain cloud-base height and temperature criteria for the existence of liquid or ice clouds (e.g., Rogers and

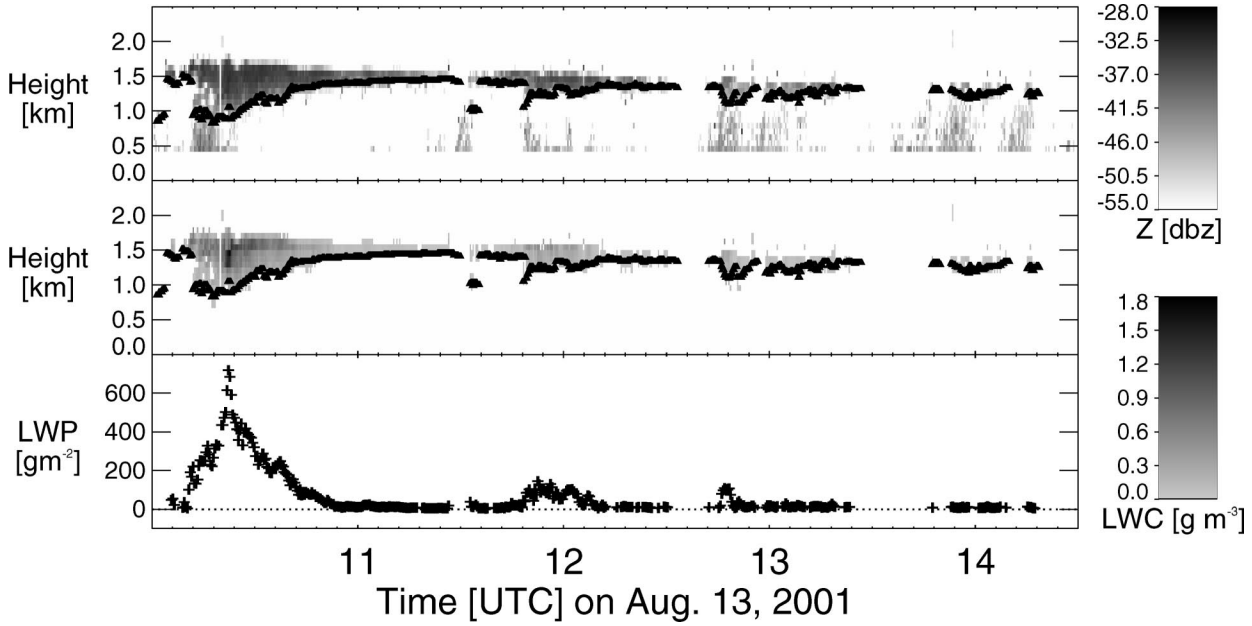

FIG. 5. Time series of (top) radar reflectivity, (center) IPT-LWC on radar resolution, and (bottom) vertically integrated LWC (LWP) 1 Aug 2001 at Cabauw, Netherlands. The black triangles in the upper two panels indicate the lidar-ceilometer cloud base.

Yau 1989) are included to minimize the ambiguities. In case of pure ice existing above pure liquid in one profile, the IPT is applied, because the microwave TB are insensitive to ice. However, in the cases of mixed phase together with pure liquid, the IPT cannot be applied since the radar reflectivity contribution for the pure liquid class cannot be isolated. Multiple liquid cloud layers impose no restriction on the IPT applicability. Last, in the case of a liquid cloud, the radar Doppler velocity is used to exclude drizzling and significantly precipitating cases. Here drizzle is assumed if the Doppler velocities are larger than 1 m s^{-1} (toward the radar) and significant precipitation when the Doppler velocities are larger than 2 m s^{-1}.

If all of the previously mentioned limiting factors are accounted for, the IPT can be applied to approximately 10% of the total time MIRACLE measured. Because MIRACLE only operated during working hours this corresponds to ~31 h of total radar measurement time. More information on the IPT-processed time series and on the data availability can be obtained on the Internet at the CLIWA-NET homepage (http://www.knmi.nl/samenw/cliwa-net/).

c. Retrieval example

An example of a retrieved LWC time series with a relatively thick cumulus cloud observed from 1000 to 1100 UTC 1 August 2001 with LWC values of up to 1.8 g m^{-3} and LWP values peaking at 700 g m^{-2} is shown in Fig. 5. Afterward, from 1100 to 1400 UTC, only scattered clouds with much less water content occur. Because of the cloud detection scheme by lidar-ceilometer and radar measurements, the IPT sets LWP to zero if no cloud is present, whereas the statistical algorithms can generate negative LWP in cloud-free cases or even in cases with very thin clouds. The retrieved temperature and humidity profiles together with the corresponding radiosonde measurements are shown in Fig. 6. The temperature profile and especially the inversion are captured adequately and the basic characteristics of the absolute humidity profile are also retrieved and are as good as expected.

6. Accuracy assessment

As stated earlier, the matrix $\mathbf{S}_{op}$ [Eq. (7)] is part of the optimal estimation solution and must be used when analyzing the accuracy of the IPT. Additionally we have investigated the impact toward the chosen microwave absorption model.

a. Theoretical accuracies

As denoted in section 3a, each retrieved profile consists of an optimal estimate and a corresponding error covariance matrix, which encompasses the theoretical retrieval error. The mean temperature and humidity errors averaged over all applicable pure liquid BBC cases are shown in Fig. 7. These errors denote the mean of the square roots of the diagonal components of the error covariance matrices $\mathbf{S}_{op}$. If the assumed errors of measurement and forward model are correct, these values should give a reliable accuracy estimate. Throughout the troposphere the temperature error is on the order of 0.5–1 K. The humidity error varies between 0.5 and

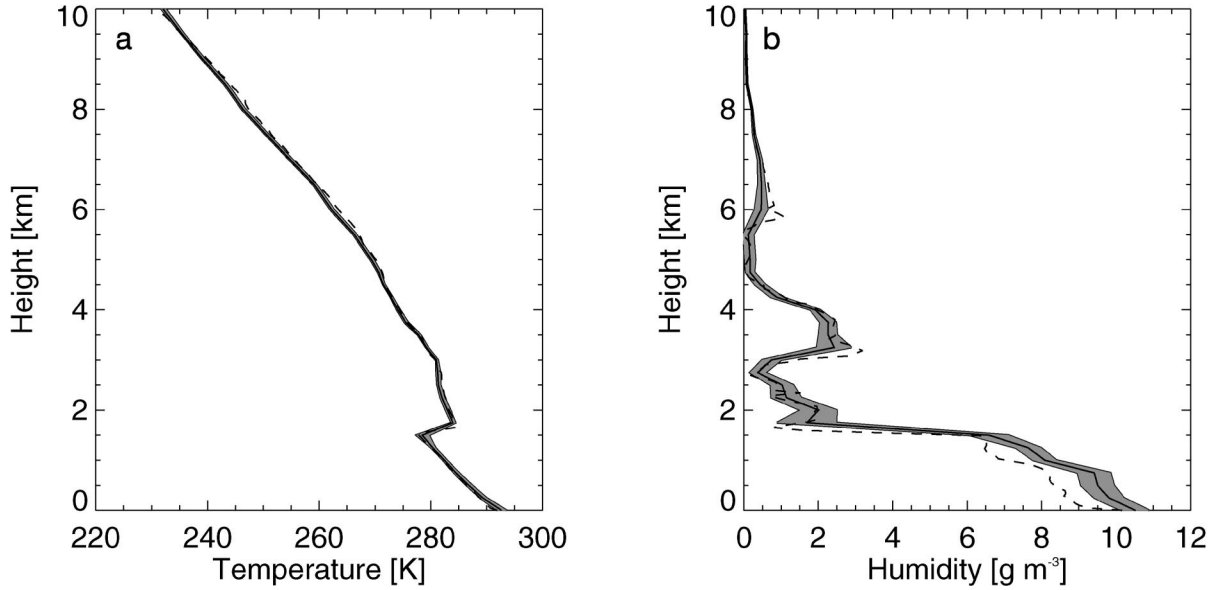

FIG. 6. Mean values of (a) temperature and (b) humidity derived during the time series shown in Fig. 5. The shaded areas denote the retrieval std dev during the time series. Also shown is the De Bilt radiosonde (dashed) from 1200 UTC.

1 g m^{-3} below 4 km and then decreases monotonically because of the exponential decay of water vapor density with height. A further important feature highlighted by Fig. 7 is the retrieval error that would result if only radiosonde statistics were used to derive temperature and humidity profiles. On average the application of remote sensing improves the theoretical accuracy of the temperature profile from 1 to 0.63 K (37%) and of the humidity profile from 1.11 to 0.64 g m^{-3} (42%) in the lowest 3 km of the troposphere. It must be stressed that these results are derived from cloudy (nonprecipitating) cases only and thus clearly show the potential of passive microwave remote sensing in comparison with infrared or optical methods, where signals attenuate in the lowest part of the liquid cloud. Also shown in Fig. 7 are the systematic deviations between the interpolated De Bilt radiosonde (a priori information) and the IPT retrieval. As expected the values for T (Fig. 7a) are close to zero

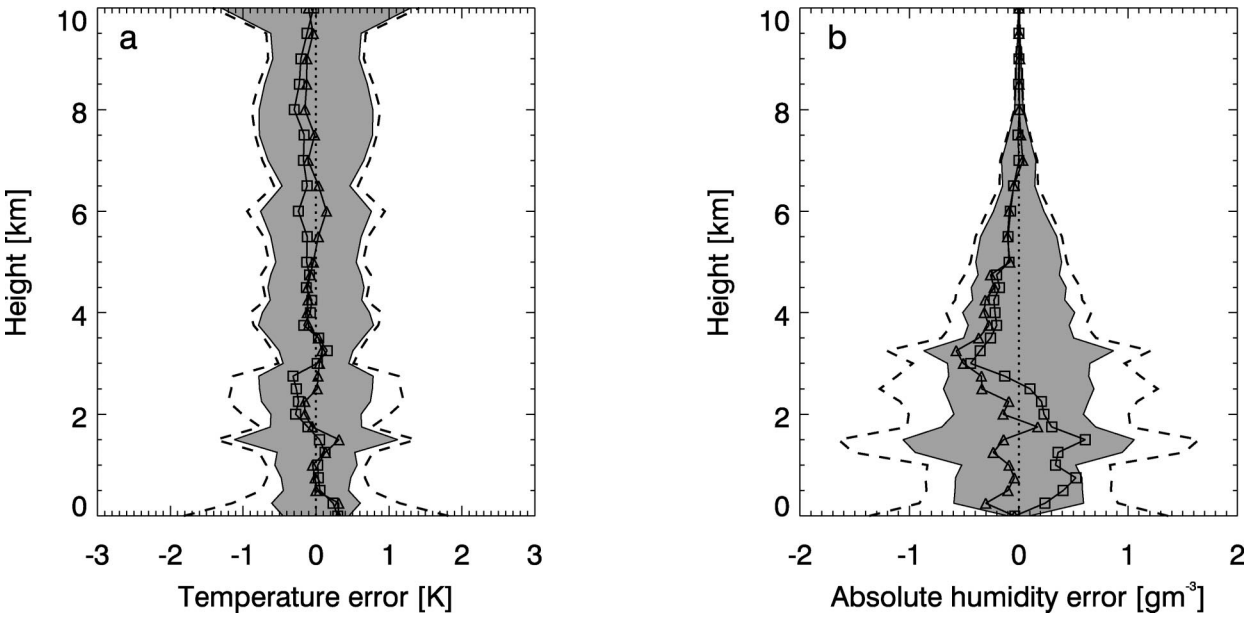

FIG. 7. Mean theoretical IPT rms errors (gray-shaded areas) derived for (a) T and (b) q for all applicable cases during the BBC campaign. Also shown are the theoretical rms errors that would be expected if only interpolated radiosondes were used (dashed lines). The squares (triangles) show the systematic differences to the interpolated De Bilt radiosonde profile assuming the gas absorption model R98 (L93).

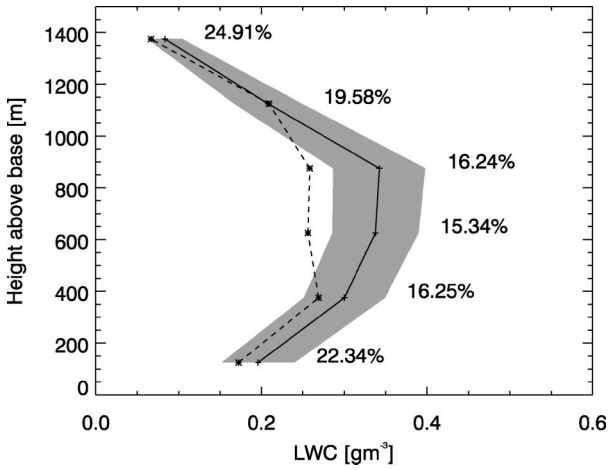

FIG. 8. Mean values of LWC derived from IPT application (solid line) to liquid clouds with a vertical extent of 1500 m (139 IPT retrievals on 23 different BBC days). The vertical coordinate is height above base. The gray-shaded area denotes the theoretical IPT-LWC errors, and the numbers show the corresponding mean relative error in percent. Additionally shown is the mean LWC profile of the retrieval constraining the *Z*–LWC relation to the statistically derived MICCY-LWP (dashed line).

with an rms difference of 0.21 K between the systematic deviations and the zero line up to a height of 3 km. The systematic deviations in humidity between the interpolated De Bilt radiosonde (a priori) and the IPT retrieval profile (Fig. 7b) are somewhat larger (rms difference of 0.35 g m^{-3} between the systematic deviations and the zero line below 3 km) whereas, again, this difference should be ideally zero. Possible influences of the gas absorption model are discussed in section 6b.

The mean LWC profile for liquid water clouds with a vertical extent of 1500 m retrieved from all applicable BBC cases is shown in Fig. 8. The relative accuracies are shown to be on the order of 15%–25%. Also shown in Fig. 8 is the mean LWC profile derived when using the *Z*–LWC relation constrained to the MICCY-LWP (section 4b). The mean IPT profile shows a more realistic curve in the sense that adiabatically rising parcels apparently lead to a significant increase in LWC in the lowest four levels, whereas the constrained relation more or less follows the *Z* profile (not shown) leading to approximately constant LWC values in the center of the cloud. The top two layers are dominated by cloud-top entrainment such that LWC decreases with height. Note that the highest layer may not be totally filled by a cloud, as the original radar reflectivities are averaged to the 250-m grid. The mean difference in LWP between both retrievals is 57 g m^{-2}. Roughly one-half of this value can be attributed to differences in the absorption model because the MICCY-LWP is derived using the L93 gas absorption model. The remaining discrepancy is probably due to the statistical error induced by the MICCY-LWP algorithm (Löhnert and Crewell 2003) or possible calibration offsets in the MICCY channels used in the IPT but not in the statistical algorithm.

b. Sensitivity to the absorption model

Because no independent evaluations of microwave absorption models exist, the IPT is now applied to the BBC data using the L93 absorption model. First we compare the systematic differences of vertically integrated *q* (IWV) between the IPT runs and the De Bilt a priori profiles. In the case of R98, this systematic difference is equal to $+0.13$ kg m^{-2}, whereas the L93 case shows a bias of -1.24 kg m^{-2}. As shown clearly in Fig. 7b, systematic differences in *q* at different heights of the R98 results cancel out in terms of IWV, whereas L93 results show a constant negative offset. Apparently the different gas absorption models can give rise to mean *q* differences of up to 0.7 g m^{-3} in the lowest 3 km. The significant differences caused by the two absorption models make one thing clear: The theoretical improvements in rms accuracy gained by adding remote sensing measurements to the radiosonde statistics (Fig. 7) must be interpreted with care because systematic differences due to the gas absorption model may cause errors in the same order of magnitude as the theoretical accuracies.

The mean differences between the R98 and L93 *T* retrievals are less than 0.3 K in all layers below 3 km (Fig. 7a). This indicates a similar oxygen absorption in both L93 and R98 models. The systematic difference in LWP between the two IPT runs is equal to -12.7 g m^{-2} (L93 − R98). Although we use the same absorption models for liquid in both IPT runs, this difference can be expected just because of the difference in gaseous absorption.

Because we do not know the truth and that possible instrument calibration offsets (microwave radiometer, radiosonde) cannot easily be accounted for, it is momentarily not possible to judge which absorption model is superior. IPT application to further measurement campaigns employing different microwave profilers may help in this respect. The differences shown here should only be used as an error indication; for instance, these offsets should be kept in mind as possible errors, as long as no reliable absorption model exists. In addition, it must also be stated that liquid water absorptions models are also subject to systematic uncertainties, especially at temperatures around and below 0°C (Westwater et al. 2001).

7. Conclusions

Integration of remote and in situ measurements can lead to improved accuracies of *T*, *q*, and LWC profiles when combined within an optimal estimation framework. A major advantage of the proposed IPT is that profiles of temperature, humidity, and cloud liquid water are retrieved simultaneously and are physically consistent in terms of different measures. For instance the

forward-modeled brightness temperatures are constrained to the measured values, the retrieved T and q profiles meet the ground-level measurements, and the q profile fulfills the condition of saturation within the detected cloud boundaries. Realistic a priori profiles of T, q, and LWC further improve the results by reducing the degrees of freedom of the underdetermined inversion problem. However, the IPT humidity retrieval results show systematic errors depending highly on the chosen gas absorption model. This underlines the fact that successful microwave remote sensing is only possible if advances in absorption models are made in the near future. A further advantage in terms of LWC profile retrieval is the independence of the IPT of statistical LWP retrieval errors, which are usually on the order of 20%–30% for two-channel microwave radiometers, not including absorption model uncertainties. This means that the vertical integral of the IPT-LWC must thus be regarded as an advanced LWP product.

These improvements distinguish the IPT from the more simple (and common) atmospheric profiling methods (e.g., when the microwave-derived LWP is used to scale the Z profile to obtain LWC). It is clear that the retrieval of atmospheric profiles in a physically consistent manner using as much information as possible should be the ultimate objective. However, it should be mentioned that the computation time (calculation of a profile takes ~30 s on a standard PC) and the computational effort of the IPT are substantially increased in comparison with simple methods. To obtain the most accurate retrievals, the assumptions concerning the covariance estimates must be carefully adjusted for different locations and different instruments. In this regard, the simple methods may be of advantage if quick results for different stations and long time series are required. However, after the successful implementation of the IPT for a certain location, the simpler methods will be outperformed.

In a next step we will incorporate measurements encompassing other spectral ranges. Including the lidar-ceilometer backscatter profile and its forward model instead of using only the cloud-base information, will allow us to infer cloud parameters such as droplet number concentration or LWC at least at the lowest cloud level. In a similar way an additional infrared sensor can be included. Another extension to be looked into is the inclusion of higher microwave frequencies (e.g., around 150 GHz) that attenuate sooner within the cloud than the MICCY frequencies. Thus, information on vertical solution of cloud liquid water may be obtained from the microwave measurements.

Current atmospheric research proposals and ongoing projects focus on the establishment of a number of integrated observation sites with a selection of different remote and in situ observation instruments. We believe that the IPT presents a first major step for integrating arbitrary measurements and combining them to form a product that increasingly resembles reality. The methodology can be extended toward drizzle, ice clouds, mixed-phase clouds, or even significantly precipitating cases. Other instruments exist that could be incorporated as additional constraints; they include wind profilers, RASS systems, or Raman lidar technology. The main future goal is to develop an ''all encompassing'' algorithm that can take into account all instruments operating momentarily at a specific station and deliver online the best estimates of profiles of temperature, humidity, and cloud hydrometeors during all weather conditions to improve weather forecasting and data assimilation techniques.

Acknowledgments. This work was made possible through the European fifth framework project CLIWA-NET (EVK2-CT-1999-00007). Special thanks go to the members of the CLIWA-NET BBC community, whose measurements contributed to the results of this paper. Especially we thank Markus Quante and Henriette Lemke from GKSS for providing the radar data and Wim Hovius (KNMI) from the Cabauw facility for providing an excellent measurement infrastructure during the BBC campaign.

REFERENCES

Crewell, S., and U. Löhnert, 2003: Accuracy of cloud liquid water path from ground-based microwave radiometry, 2. Sensor accuracy and synergy. *Radio Sci.*, **38**, 8042, doi:10.1029/2002RS002634.

——, H. Czekala, U. Löhnert, T. Rose, C. Simmer, R. Zimmermann, and R. Zimmermann, 2001: Microwave radiometer for cloud cartography: A 22-channel ground-based microwave radiometer for atmospheric research. *Radio Sci.*, **36,** 621–638.

——, A. Feijt, E. van Meijgard, and C. Simmer, 2003: CLIWA-NET BALTEX BRIDGE Cloud Liquid Water Network. International BALTEX Secretariat Publ. 26, 53 pp.

Danne, O., M. Quante, D. Milferstädt, H. Lemke, and E. Raschke, 1999: Relationships between Doppler spectral moments within large-scale cirro- and altostratus cloud fields observed by a ground-based 95-GHz cloud radar. *J. Appl. Meteor.*, **38,** 175–189.

Frisch, A. S., C. W. Fairall, G. Feingold, T. Utal, and J. B. Snider, 1998: On cloud radar and microwave radiometer measurements of stratus cloud liquid water profiles. *J. Geophys. Res.,* **103,** 23 195–23 197.

Han, Y., and E. R. Westwater, 1995: Remote sensing of tropospheric water vapor and cloud liquid water by integrated ground-based sensors. *J. Atmos. Oceanic Technol.,* **12,** 1050–1059.

——, J. B. Snider, E. R. Westwater, S. H. Melfi, and R. A. Ferrare, 1994: Observations of water vapor by ground-based microwave radiometers and Raman lidar. *J. Geophys. Res.,* **99,** 18 695–18 702.

Issig, C., 1997: Ein spektrales Wolkenmodell mit integriertem Strahlungsübertragungsmodell zur Unterstützung von Niederschlagsalgorithmen. Ph.D. dissertation, University of Bonn, 119 pp. [Available from Meteorological Institute, University of Bonn, Auf dem Hügel 20, 53121 Bonn, Germany.]

Janssen, M. A., 1993: *Atmospheric Remote Sensing by Microwave Radiometry.* Wiley Series in Remote Sensing, John Wiley and Sons, 572 pp.

Kuhn, T., 2003: Atmospheric absorption models for the millimeter wave range. Ph.D. dissertation, University of Bremen, 192 pp. [Available from Institute for Environmental Physics, Otto-Hahn-Allee 1, 28359 Bremen, Germany.]

Lerner, J. A., E. Weisz, and G. Kirchengast, 2002: Temperature and humidity retrieval from simulated Infrared Atmospheric Sound-

ing Interferometer (IASI) measurements. *J. Geophys. Res.*, **107,** 4189, doi:10.1029/2001JD900254.

Liebe, H. J., G. A. Hufford, and M. G. Cotton, 1993: Propagation modeling of moist air and suspended water/ice particles at frequencies below 1000 GHz. *Atmospheric Propagation Effects through Natural and Man-Made Obscurants for Visible through MM-Wave Radiation,* AGARD-CP-542, 3.1–3.10.

Liljegren, J. C., E. E. Clothiaux, G. G. Mace, S. Kato, and X. Dong, 2001: A new retrieval method for cloud liquid water path using a ground-based microwave radiometer and measurements of cloud temperature. *J. Geophys. Res.*, **106,** 14 485–14 500.

Löhnert, U., and S. Crewell, 2003: Accuracy of cloud liquid water path from ground-based microwave radiometry, Part I: Dependency of cloud model statistics. *Radio Sci.*, **38,** 8041, doi: 10.1029/2002RS002654.

——, ——, A. Macke, and C. Simmer, 2001: Profiling cloud liquid water by combining active and passive microwave measurements with cloud model statistics. *J. Atmos. Oceanic Technol.,* **18,** 1354–1366.

Ovtchinnikov, M., and Y. L. Kogan, 2000: Evaluation of radar retrieval algorithms in stratiform clouds using large-eddy simulations. *J. Geophys. Res.*, **105,** 17 351–17 359.

Revercomb, H. E., and Coauthors, 2003: The ARM Program's water vapor intensive observation periods—Overview, initial accomplishments, and future challenges. *Bull. Amer. Meteor. Soc.,* **84,** 217–236.

Rodgers, C. D., 2000: *Inverse Methods for Atmospheric Sounding: Theory and Practice.* World Scientific, 238 pp.

Rogers, R. R., and M. K. Yau, 1989: *A Short Course in Cloud Physics.* Butterworth-Heinemann, 290 pp.

Rosenkranz, P. W., 1998: Water vapor microwave continuum absorption: A comparison of measurements and models. *Radio Sci.*, **33,** 919–928.

Simmer, C., 1994: *Satellitenfernerkundung Hydrologischer Parameter der Atmosphäre mit Mikrowellen.* Verlag Dr. Kovac, 313 pp.

Solheim, F., J. R. Godwin, E. R. Westwater, Y. Han, S. J. Keihm, K. Marsh, and R. Ware, 1998: Radiometric profiling of temperature, water vapor and cloud liquid water using various inversion methods. *Radio Sci.,* **33,** 393–404.

Stankov, B. B., 1998: Multisensor retrieval of atmospheric properties. *Bull. Amer. Meteor. Soc.*, **79,** 1835–1854.

Westwater, E. R., 1997: Remote sensing of tropospheric temperature and water vapor by integrated observing systems. *Bull. Amer. Meteor. Soc.*, **78,** 1991–2006.

——, Y. Han, M. D. Shupe, and S. Y. Matrosov, 2001: Analysis of integrated cloud liquid and precipitable water vapor retrievals from microwave radiometers during SHEBA. *J. Geophys. Res.*, **106,** 32 019–32 030.